

# Highly efficient endosomal labeling of progenitor and stem cells with large magnetic particles allows magnetic resonance imaging of single cells

Kathleen A. Hinds, Jonathan M. Hill, Erik M. Shapiro, Mikko O. Laukkanen, Alfonso C. Silva, Christian A. Combs, Timothy R. Varney, Robert S. Balaban, Alan P. Koretsky, and Cynthia E. Dunbar

**Tracking transplanted stem cells using magnetic resonance imaging (MRI) could offer biologic insight into homing and engraftment. Ultrasmall dextran-coated iron oxide particles have previously been developed for uptake into cells to allow MRI tracking. We describe a new application of much larger, micron-scale, iron oxide magnetic particles with enhanced MR susceptibility, which enables detec-**

**tion of single cells at resolutions that can be achieved in vivo. In addition, these larger particles possess a fluorophore for histologic confirmation of cell distribution. We demonstrate highly efficient, non-toxic, endosomal uptake of these particles into hematopoietic CD34<sup>+</sup> cells and mesenchymal stem cells documented by confocal and electron microscopy. Labeled cells retain biologic activity with**

**preservation of colony-forming ability and differentiation capacity. MRI studies could detect labeled CD34<sup>+</sup> cells and mesenchymal stem cells (MSCs) at single cell resolution. This appears to be a promising tool for serial noninvasive monitoring of in vivo cell homing and localization using MRI. (Blood. 2003;102:867-872)**

© 2003 by The American Society of Hematology

## Introduction

Cell therapy, or the administration of autologous or allogeneic ex vivo manipulated human cell suspensions for regeneration of various organs or tissues, is being explored as a potential approach to a wide variety of degenerative, malignant, or genetic diseases. Transplantation of hematopoietic stem cells to rescue bone marrow function following high-dose myeloablative therapy for leukemias, aplastic anemia, or other hematologic disorders has profoundly impacted the course of these previously lethal disorders for the past 30 years; however, the factors governing the ability of primitive hematopoietic stem cells to home to the marrow microenvironment following transplantation are poorly understood.<sup>1</sup> More recently, hematopoietic stem cells and marrow-derived mesenchymal stem cells have been reported to have the ability to participate in, or stimulate the regeneration of, diverse tissues and organs, including liver, myocardium, endothelium, and brain.<sup>2-7</sup> Much of this work has thus far been carried out in animal models, but clinical trials to investigate the safety and efficacy of novel cell therapies have begun.

The ability to noninvasively track cells in vivo, following either local injection or intravenous administration, would provide insights into many basic and practical questions regarding these cell therapies. Hematopoietic progenitor cells have been labeled with membrane dyes and recovered from informative sites such as the marrow and spleen following intravenous administration in murine models, but membrane dyes or other fluorescent labels require tissue sampling for detection, preventing real-time noninvasive tracking, except at very low resolution using new highly sensitive optical cameras.<sup>8,9</sup> Nuclear medicine techniques and positron emission tomography (PET) scanning are under active develop-

ment but likely will never reach levels of sensitivity and resolution necessary for detection of small cell numbers or localization of these cells anatomically within organs.<sup>10</sup> Magnetic resonance imaging has the potential to overcome these obstacles, by allowing serial noninvasive monitoring of administered cell populations, if cells can be made detectable via contrast agent loading.<sup>11</sup>

We now describe a novel intracellular contrast agent that is taken up by stem and progenitor cells and incorporated into perinuclear endosomes without affecting cell proliferation or functional capabilities. The magnetic resonance imaging (MRI) contrast derives from a micron-scale particle that is an aggregate of iron oxide magnetite mixed with a fluorophore and encased within an inert polymer shell. We found that a wide variety of primary cells with therapeutic potential, including hematopoietic progenitor (CD34<sup>+</sup>) and mesenchymal stem cells (MSCs), could be efficiently labeled with this particle with preservation of biologic activity. Uptake of this agent allowed MRI detection of single cells.

## Materials and methods

### Superparamagnetic particles

Superparamagnetic divinyl benzene inert polymer microspheres were obtained from Bangs Laboratories (Fishers, IN). The average size of each microparticle is 0.9  $\mu$ m. The particles contain a magnetite iron oxide component (63.4%) as well as a fluorescein-5-isothiocyanate analog (Dragon Green) component trapped within the polymer matrix. Both of the components were added to the particle by swelling the cage matrix with an organic solvent, adding the fluorophore and as much iron oxide as possible,

From the Hematology Branch, Laboratory of Molecular Biology, Laboratory of Cardiac Energetics, and Light Microscopy Core Facility, National Heart, Lung, and Blood Institute (NHLBI), National Institutes of Health, Bethesda, MD; Laboratory of Functional and Molecular Imaging, National Institute of Neurologic Disorders and Stroke, National Institutes of Health, Bethesda, MD; and Osiris Therapeutics, Baltimore, MD.

Submitted December 4, 2002; accepted March 12, 2003. Prepublished online as *Blood* First Edition Paper, April 3, 2003; DOI 10.1182/blood-2002-12-3669.

K.A.H. and J.M.H. contributed equally to this work.

**Reprints:** Cynthia E. Dunbar, Molecular Hematopoiesis Section, Hematology Branch, National Heart, Lung, and Blood Institute, National Institutes of Health, Bldg 10, Rm 7C103, 9000 Rockville Pike, Bethesda, MD 20892.

The publication costs of this article were defrayed in part by page charge payment. Therefore, and solely to indicate this fact, this article is hereby marked "advertisement" in accordance with 18 U.S.C. section 1734.

© 2003 by The American Society of Hematology

and then shrinking the matrix back to the average size of 0.9  $\mu\text{m}$  by removing the solvent and replacing it with a sterile aqueous solution. Particles were prepared for target cell exposure by washing with phosphate-buffered saline (PBS) after immobilization of the particles using a magnet and then resuspension at a concentration of 1% weight per volume sterile PBS. The iron content of this suspension is approximately 4.56 mg/mL.

The particle suspension was stored at 4°C and gently resuspended prior to labeling procedures.

For in vitro comparisons on the effects of the size of particles on MR images, dilutions of ferumoxides (Feridex; Berlex Laboratories, Wayne, NJ), an FDA-approved iron oxide nanoparticle, were used. This particle consists of a single nanocrystal of iron oxide, with a 7- to 10-nm diameter and coated with dextran. Bangs particles and ferumoxides particles were used at iron concentrations of 1.0, 0.5, 0.2, 0.1, and 0.01 mM in 2% agarose in small culture tubes. The culture tubes were then themselves embedded in 2% agarose in a small beaker to ameliorate susceptibility effects around the tubes. The sample ensemble was placed inside a 3.5-cm diameter, 8.5-cm long Bruker Biospin (Billerica, MA) birdcage coil. Two-dimensional MRI was then performed with the following imaging parameters: echo time (TE) = 7 milliseconds, repetition time (TR) = 4000 milliseconds, field of view (FOV) = 6  $\times$  6 cm, slice thickness = 2 mm, matrix = 512  $\times$  512, number of excitations acquired (NEX) = 1, bandwidth (BW) = 101 kHz, and total imaging time = 34 minutes. These parameters yielded a pixel size of 117  $\times$  117  $\times$  2000  $\mu\text{m}$ . To calculate relaxivity, samples were imaged at 8 echo times, ranging from 2 to 20 milliseconds. The calculated  $T_2^*$  (effective transverse relaxation time) values were then fit to a standard relaxivity equation. These experiments were all performed at 4.7 tesla (T) and 11.7 T on Bruker Biospin Avance Spectrometers.

### Cell culture and labeling

Peripheral blood progenitor cells were obtained by apheresis from healthy volunteers entered on an NHLBI institutional review board-approved protocol following 5 subcutaneous injections of 10  $\mu\text{g}/\text{kg}/\text{d}$  granulocyte colony-stimulating factor (G-CSF). Purified CD34<sup>+</sup> cells were obtained using the Isolex 300 Magnetic Cell Separator (Baxter, Irvine, CA) and cryopreserved. Mean purity was 85% to 95% CD34<sup>+</sup>. CD34<sup>+</sup> cells were thawed in a water bath and cultured overnight in stem cell media (SCM) consisting of Dulbecco modification of Eagle medium (DMEM), 10% fetal bovine serum (FBS), 4 mM L-glutamine, 50 mg/mL penicillin and streptomycin, and 100 ng/mL each of recombinant human Flt-3 ligand (Immunex, Seattle, WA), stem cell factor (SCF; Amgen, Thousand Oaks, CA), and megakaryocyte growth and development factor (MGDF; Amgen). CD34<sup>+</sup> cells were seeded at a concentration of 500 000 cells per well in 200  $\mu\text{L}$  SCM in a 96-well plate, and the particle suspension was added to each well and cultured for 1 to 18 hours at 37°C in 5% CO<sub>2</sub>. Cells were then removed from the wells, washed 3 times via centrifugation at 1500 rpm, and analyzed.

Primary porcine bone marrow MSCs were derived from bone marrow aspirates obtained from healthy adult farm swine. Aspirates were diluted with 2 volumes of PBS, washed, and the mononuclear cells isolated by density gradient centrifugation (Ficoll-Paque; Amersham-Biosciences, Piscataway, NJ). Recovered cells were washed twice in PBS and resuspended in mesenchymal stem cell growth medium (MSCGM) (Poetics, Biowhitaker, Walkersville, MD) supplemented with MSCGM bullet kits (Poetics). Cells were then seeded at a concentration of 1000/mm<sup>2</sup> in supplemented MSCGM. After 5 days nonadherent cells were removed and adherent colonies expanded further in culture. For MSC labeling iron oxide particle suspension (10  $\mu\text{L}/\text{mL}$ ) was added to nonconfluent MSCs and incubated for 4 to 18 hours at 37°C in 5% CO<sub>2</sub>. Excess particles were removed by washing with PBS, and the cells were analyzed or continued in culture.

### Hematopoietic colony culture

Following particle exposure at a concentration of 0 to 25  $\mu\text{L}/\text{mL}$  for 18 hours, CD34<sup>+</sup> cells were plated in duplicate in standard semisolid methylcellulose hematopoietic progenitor culture media (human MethoCult+GF; Stem Cell Technologies, Vancouver, BC) at concentrations from 5  $\times$  10<sup>2</sup> to 5  $\times$  10<sup>4</sup>/mL. These culture plates were incubated at

37°C in 5% CO<sub>2</sub>. Colonies consisting of more than 50 cells were identified and enumerated 12 to 14 days later.

### Proliferation and differentiation assays

Labeled MSC viability was assessed by trypan blue exclusion (data not shown) and in vitro proliferation using a modified MTT assay (3-[4,5-dimethylthiazol-2-yl]-2,5-diphenyl tetrazolium bromide) (Roche Diagnostics, Indianapolis, IN). Briefly, 1000 MSCs per well of a 24-well plate were seeded at early passage (P3-P5) and growth curves established after overnight labeling with a range of particle concentrations (0.1-50  $\mu\text{L}/\text{mL}$ ). Particles were either removed by repeated washing and replaced with fresh media or left in the media for the duration of the assay.

Quadruplicate samples were assayed at each time point and the experiment was repeated in triplicate.

For osteogenic differentiation of porcine MSCs, cells were maintained in 6-well plates for 17 days in the presence of osteogenic supplements as previously described.<sup>12</sup> Prior to staining for calcium deposition or alkaline phosphatase activity, sample wells were rinsed with Tyrode solution (9.72 g Tyrode salts, 1.0 g NaHCO<sub>3</sub> per liter), fixed in 10% formalin for 1 hour at room temperature, and then rinsed twice with distilled water. To identify calcium deposition by the von Kossa method, 2% AgNO<sub>3</sub> was added to fixed samples. Following a 10-minute incubation period in the dark, samples were rinsed 3 times with distilled water, exposed to bright light for 15 minutes, and then rinsed with distilled water. Samples were dehydrated by a final rinse with 100% ethanol and allowed to air dry before photographing. To stain for alkaline phosphatase activity, 1 mL Fast Violet-naphthol solution (Sigma [St Louis, MO] Kit 85L-3R, prepared according to manufacturer's instructions) was added to each sample fixed as described above. Samples were left for 1 hour in darkness, rinsed with distilled water, and photographed.

### Confocal microscopy

Cells used for confocal microscopy were incubated with or without the microparticle and other cellular stains that contrast with the Dragon Green color wavelength. Cells that were incubated in Cell Tracker Orange (Molecular Probes, Eugene, OR) were first washed with warm PBS and then adhered to a poly-L-lysine coverslip for 30 minutes at 37°C, 5% CO<sub>2</sub>. Following incubation, cells were gently rinsed with warm PBS 3 times. The coverslip was then covered with an adhesive confocal coverwell (Grace Bio-Labs, Bend, OR) and filled with warm PBS. All imaging experiments were conducted using a Zeiss LSM 510 confocal microscope and a C-Apochromat 63 $\times$ , 1.2 numerical aperture lens. Dragon Green and Cell Tracker Orange were imaged sequentially using 488- and 543-nm excitation light and 505- to 530- and 560- to 615-nm bandpass filters, respectively. The pinholes on the emission channels were set on all experiments to produce an optical slice thickness of 1.5  $\mu\text{m}$ . Images were acquired sequentially, and bandpass emission filters were used to avoid spectral bleed-through between the imaging channels. For MSC imaging, after washing off nonendocytosed particles, cells were seeded at varying concentrations into 2-well glass-bottomed chamber slides. To confirm endosomal uptake, CM-DiI (3',3'-dioctadecyl-5-5'-di(4-sulfophenyl)-oxocarbocyanine, sodium salt; Molecular Probes) and DAPI (4',6'-diamidino-2-phenylindole; Molecular Probes) for nuclear counterstain were added as per manufacturer's instructions.

### Electron microscopy

One million cells were initially fixed with 1.25% glutaraldehyde in 0.1 M cacodylate buffer (containing 0.1 M sodium cacodylate trihydrate, 0.4 mL hydrochloric acid, and 0.05% calcium chloride at a pH of 7.4 for a total of 1 L) at 4°C overnight. After washing in Sabatini solution (0.1 M cacodylate buffer containing sucrose and calcium chloride) the cells were postfixed in 1% osmium tetroxide, dehydrated through ascending alcohol and propylene oxide, and embedded in SCI Poxyl 812 (Energy Beam Sciences, Agawam, MA). Ultrathin sections were cut with a Leica Ultracut UCT, stained with uranyl acetate and lead citrate, and examined with a JEOL 1200 EXII transmission electron microscope.

## Cellular MRI

Cellular imaging was performed on an 11.7-T Bruker Avance Spectrometer. Two chamber culture dishes with live cells in culture media were placed inside a 3.5-cm diameter, 8.5-cm long Bruker birdcage coil. After appropriate image localization scans, a high-resolution, 3-dimensional gradient echo pulse sequence was run on the entire sample. Imaging parameters were as follows: TE = 4 milliseconds, TR = 200 milliseconds, FOV =  $5 \times 3 \times 0.2$  cm, matrix =  $512 \times 512 \times 40$ , NEX = 4, and BW = 101 kHz, total imaging time = 4.5 hours. These parameters yielded a voxel size roughly of  $100 \times 50 \times 50 \mu\text{m}$ .

## Results

### Large particles compared with nanoparticles

We compared the magnetic susceptibility effect of these particles to previously utilized nanoparticles such as ferumoxides (Figure 1). Calculated  $R_2^*$  relaxivities at 4.7 T for the ferumoxides were  $240 \pm 27 \text{ mM}^{-1} \text{ s}^{-1}$  and for the Bangs particles was  $356 \pm 21 \text{ mM}^{-1} \text{ s}^{-1}$ . At 11.7 T, the relaxivities are increased, with ferumoxides being  $498 \pm 19 \text{ mM}^{-1} \text{ s}^{-1}$  and the Bangs particles being  $851 \pm 62 \text{ mM}^{-1} \text{ s}^{-1}$ . This is consistent with the current body of theory work that  $R_2^*$  relaxivities are field dependent. With equal iron content, the larger particles yielded darker images under  $T_2^*$ -weighted imaging conditions. The relaxation enhancement as a percent difference between small and large particles is greatest with highest iron concentrations; however, the highest magnitude difference occurred with an intermediate concentration. The amplification effects of the large particles with respect to the small particles are clearly evident down to concentrations of  $100 \mu\text{M Fe}$ .

Normalized to iron content, the larger Bangs particles greatly decrease  $T_2^*$  and enhance the susceptibility effect in the images, as seen in the direct comparison data. While the total iron content of the Bangs and ferumoxides samples were kept equal, the sizes of the particles were different. Ferumoxides has a 10-nm core, while the effective magnetite core size of the Bangs particles used for this experiment was 760 nm. This results in nearly 5000-fold fewer Bangs particles than ferumoxides particles in each comparison tube. If we were to normalize the MR effects to the number of particles, this disparity would be much greater.

### Labeling efficiency and microscopy

CD34<sup>+</sup> cells were exposed to various concentrations of the particle. CD34<sup>+</sup> primary hematopoietic cell populations include primitive lineage-committed progenitor cells and true long-term repopulating stem cells able to fully reconstitute patients following myeloablation and autologous or allogeneic stem cell transplantation.<sup>13</sup> These cells were chosen as a representative nonadherent cellular target. Incubation with particles for 12 to 18 hours at concentrations

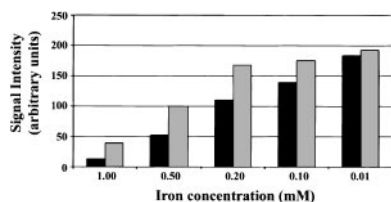


**Figure 1. In vitro relaxometry characteristics of iron particles.** Dilutions of ferumoxides 10-nm particles (light gray bars) and Bangs 0.9- $\mu\text{m}$  particles (relative size of magnetite core is 760 nm; dark gray bars) were prepared in 2% agarose gels. The final concentration of iron particles is given on the x-axis, and the signal intensities of  $T_2^*$ -weighted images are shown on the y-axis. These are data acquired at 4.7 T with a TE of 7 milliseconds.

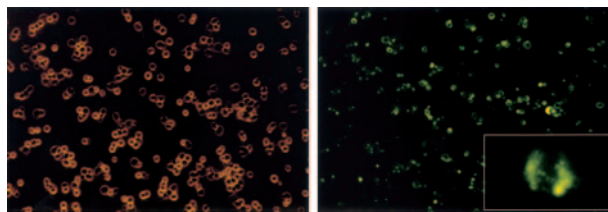


**Figure 2. Labeling of human peripheral blood CD34<sup>+</sup>.** Human primary CD34<sup>+</sup> cells were seeded at a concentration of 500 000 cells in 200  $\mu\text{L}$  stem cell media; 1  $\mu\text{L/mL}$  fluorescent particle suspension was added to the well, and the cells were incubated at 37°C for 18 hours. The cells were collected, washed, and resuspended on a chamber slide for microscopy. The left panel shows light microscopy images of the cells, showing a uniform population of primitive hematopoietic progenitors with no evidence of toxicity and some cells undergoing active cell division; original magnification,  $\times 100$ . The right panel is a fluorescent micrograph of the same field, showing that more than 90% of the cells fluoresce green, with relatively homogeneous intensity; original magnification,  $\times 100$ . The inset is a higher-power view ( $\times 1200$ ) of a fluorescent cell in the midst of mitosis, with segregation of the label occurring to both daughter cells.

down to 2.5  $\mu\text{L/mL}$  resulted in homogeneous labeling of more than 90% of these cells (Figure 2) with equal segregation of intracellular particles with each cellular division (Figure 2, insert). Labeling periods as brief as 1 hour resulted in similar labeling efficiencies and intensity, indicating rapid uptake. Primary human peripheral blood lymphocytes could also be labeled with similar efficiencies (data not shown). Confocal fluorescence microscopy (Figure 3A) revealed a cytoplasmic granular distribution of the particles within the CD34<sup>+</sup> cells. Electron microscopy showed striking uptake of the large iron oxide particles, with encasement of the particles within membrane-bound organelles (Figure 3B).

To further demonstrate labeling efficiency, porcine primary bone marrow-derived mesenchymal stem cells (MSCs) were chosen as a representative adherent cell population. MSCs can be expanded extensively in vitro and induced to differentiate into a variety of mesenchymal tissues, including fat, cartilage, and bone.<sup>12,14</sup> Overnight exposure of MSCs to 10  $\mu\text{L/mL}$  of particles resulted in efficient labeling with localization at high densities in perinuclear cytoplasm. Comparison of particle with CM-Dil labeling confirmed endosomal uptake (Figure 4).

### Preservation of proliferation and differentiation

The growth characteristics of primitive hematopoietic colonies (colony-forming units [CFUs]), consisting of hundreds to thousands of differentiated cells derived from single labeled CD34<sup>+</sup> cells, were assessed following particle exposure at concentrations from 1 to 25  $\mu\text{L/mL}$  for 18 hours. CFU number and proliferative capacity were not significantly altered, nor was the lineage commitment of each individual progenitor, because the colonies were of normal size and there was no change in distribution of myeloid and erythroid colonies (Figure 5A). Even after the 8 to 10 cell divisions on average required to form a CFU, the label appeared to distribute to each cell in the colony, as assessed by fluorescent microscopy.

Growth characteristics of labeled MSCs were assessed using a cell proliferation assay (Figure 5B). MSCs were not affected by 18 hours of exposure to a range of bead concentrations from 0.1  $\mu\text{L/mL}$  to 50  $\mu\text{L/mL}$ . Cell proliferation was marginally reduced if beads at effective labeling concentrations were not removed from the media for the duration of the growth assay. The segregation of the particles into membrane-bound cytoplasmic perinuclear endosomes appears to allow incredibly dense iron particle loading of cells without serious impact on other cellular processes.

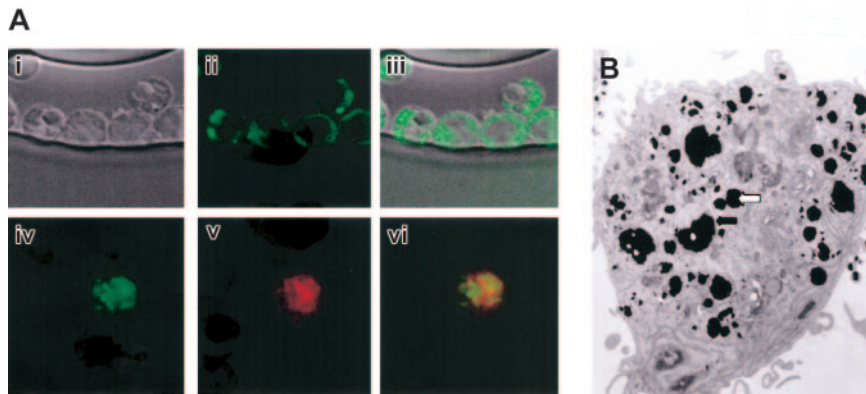


**Figure 3. Confocal fluorescent and electron microscopy of CD34<sup>+</sup> cells.** Human CD34<sup>+</sup> cells exposed to 10  $\mu$ L/mL of the iron oxide fluorescent particles for 18 hours, washed, and analyzed. (A) Depicted are phase contrast images of the CD34<sup>+</sup> cells (i) and the green fluorescence of the cells (ii). Panel Aiii shows an overlay of panels Ai and Aii. Also shown is green fluorescence from the iron oxide particles within the cell (iv) and Cell Tracker Orange fluorescence of the cytoplasm of viable cells (v). Panel Avi shows an overlay of panels Aiv and Av, demonstrating a granular distribution of the particle fluorescence throughout the cytoplasm of the cell. Original magnification for Ai-Avi,  $\times$  400. (B) Electron micrograph of single CD34<sup>+</sup> cell showing accumulation of iron particles into membrane-bound organelles (arrows indicate examples). Original magnification,  $\times$  400.

Labeled MSCs were cultured and followed by serial flow cytometry to assess the fate of the particles with multiple cell divisions. Figure 5C shows a progressive and even decrease in fluorescence per cell over time with cell divisions, suggesting even distribution of particles to daughter cells. These cells have been followed up to 3 weeks in culture after optimal labeling and can still be imaged by both confocal microscopy and MRI, indicating both that initial labeling is very dense and that even much lower numbers of particles per cell will allow imaging. This is promising for in vivo tracking of proliferative cell populations.

MSCs have been defined based on their ability to differentiate into several different mesenchymal lineages. We assessed whether the labeling process impacted on the differentiation potential of the MSCs in vitro. Osteogenic potential was identical to control MSCs, assessed by alkaline phosphatase staining (Figure 6), in addition to measurement of calcium deposition (data not shown). Differentiation to adipocytes as defined by peroxisome proliferator-activated receptor- $\gamma$  (PPAR $\gamma$ ) mRNA expression was also unaffected (data not shown).

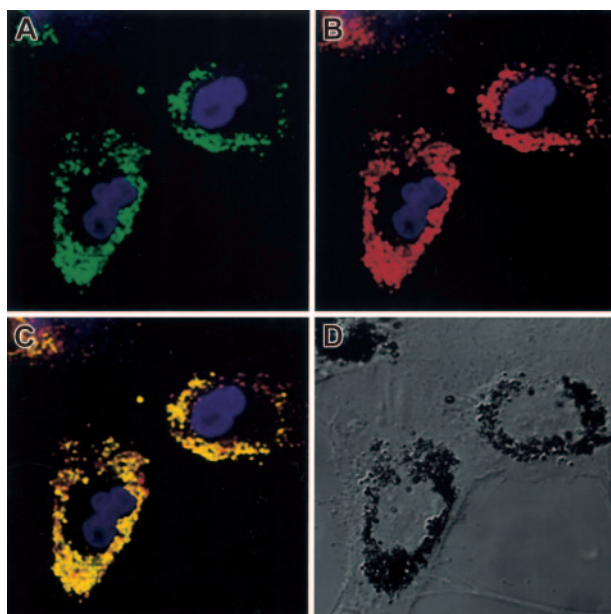


**Figure 4. Confocal fluorescent microscopy of porcine mesenchymal stem cells.** A subconfluent monolayer of primary porcine marrow MSCs were exposed to 10  $\mu$ L/mL of the iron oxide fluorescent microparticles overnight. Excess particles were washed off with PBS. (A) Green fluorescence of beads. (B) Red fluorescence of endosomal marker CM-Dil. (C) Colocalization of the 2 colors confirming endosomal particle uptake. (D) Nomarski optics view revealing the outlines of the fibroblastic cells and the iron particles clearly clustered in perinuclear organelles. Original magnification for all panels,  $\times$  100.

### Single cell MRI

Single cells could be detected in vitro using MRI with a signal void corresponding to the position of each cell. Figure 7A shows one slice from a 3-dimensional data set obtained from imaging a chamber culture dish containing live, labeled MSCs in culture media. Some spots are darker and larger than others, owing to both partial volume effects inherent in the imaging parameters and differential amounts of label incorporated into each cell. A representative confocal image (Figure 7B) showing labeled cells with DAPI nuclear counterstaining shows the efficiency of MSC labeling is almost 100%. The combination of very efficient uptake and large particle size results in greatly increased resolution on MRI. The greatest magnitude of changes involved T<sub>2</sub><sup>\*</sup>, with much less marked T<sub>1</sub> effects. The lack of a significant T<sub>1</sub> effect is expected, because the iron oxide core is shielded from the solvent.

### Discussion

The ability to localize or track specific cell populations in vivo via MRI has been pursued intensively over the past decade. A number of different contrast agents have been developed, all predicated on loading cells with paramagnetic or superparamagnetic compounds. The first such experiments used fetal rat cells harvested from sheets of cortical tissue. To label the cells, viral particles reconstituted to contain ultrasmall iron oxide particles were incubated with the fetal cell suspension. The cells were then grafted back into rat brains, with the grafts appearing dark in T<sub>2</sub>-weighted images.<sup>15</sup> Subsequent studies using impermeable paramagnetic compounds, such as Gadolinium (III)(1,4,7,10-tetraazacyclododecane-1,4,7,10-tetra(acetic acid)) (GdDOTA)-poly-D-lysine or dextran, required microinjection of the agent into individual cells. This method had useful applications in embryology, with injection of large single cells in developing embryos, but has not been practical for tracking populations of cells in whole organisms.<sup>16</sup> Initial techniques to facilitate endogenous cellular uptake of superparamagnetic iron oxide particles included targeting to the transferrin receptor via monoclonal antibodies or liposomal coating and then membrane fusion, but neither resulted in efficient enough uptake for in vivo tracking, and there was significant cellular toxicity or impact on critical cellular characteristics.<sup>17,18</sup> Small superparamagnetic iron particles coated with dextran were taken up into cells via endocytosis and allowed dynamic tracking of loaded T cells to a site of inflammation in the rat testicle<sup>19,20</sup>; this labeling enabled single

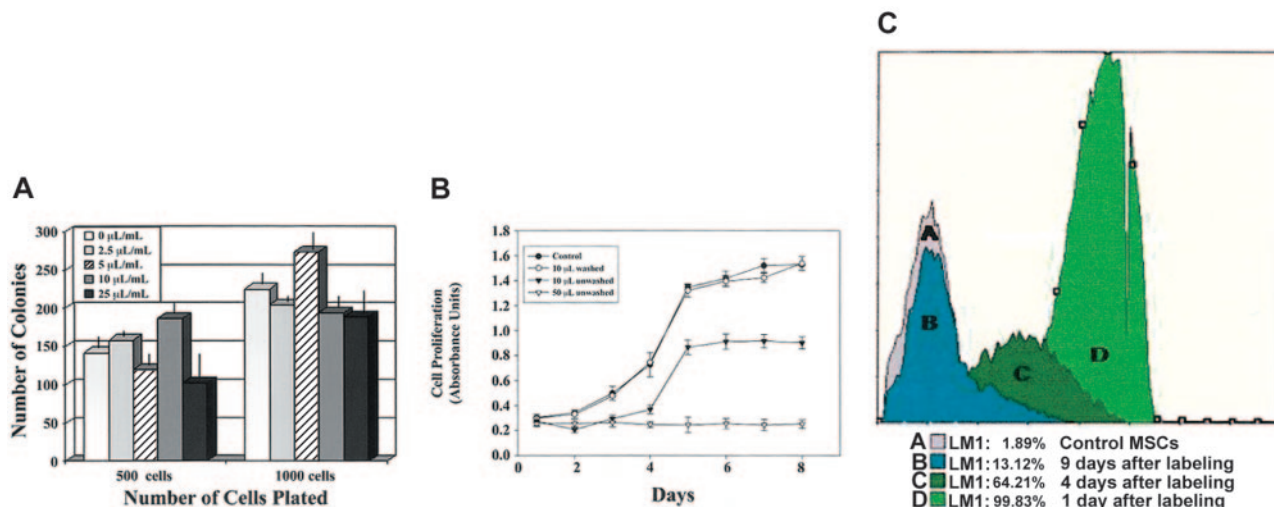


**Figure 5. Impact of particle exposure on hematopoietic progenitor proliferation and mesenchymal stem cell proliferation.** (A) CD34<sup>+</sup> human progenitor cells were exposed to a range of concentrations of the iron oxide fluorescent particle for 18 hours and then plated in methylcellulose. Ten to 12 days later, macroscopic colonies (CFUs) were enumerated. The x-axis gives the concentration of particle added following plating of either 500 or 1000 cells and the y-axis the number of CFUs present. There was no difference in the average size or composition of the individual colonies. The colony number data are derived from 3 independent experiments. These data are from 1 representative experiment; error bars show standard deviations. Similar results were obtained in 3 independent experiments using different CD34<sup>+</sup> cell donors. (B) MSCs were exposed to a range of particle concentrations and growth assessed using an MTT assay. No effect on cell proliferation was observed after overnight labeling with 1 or 10 μL/mL. Proliferation was mildly impaired if particles were not removed from the media for the duration of the growth assay. The y-axis shows cell proliferation in absorbance units at 560 nm and the x-axis days in culture; error bars show standard deviations. (C) MSCs were exposed to 10 μL/mL particles for 4 hours, and the particles were removed. The next day, and then serially for up to 10 days, aliquots of the cells were collected and analyzed by flow cytometry for the presence of the fluorescent particles. The histograms show the uniform very bright initial labeling, with gradual decline over the next 10 days with ongoing cell proliferation.

cells to be detected in vitro. Using the same approach, oligodendrocyte precursors have been labeled with small dextran superparamagnetic iron particles and localized after infusion into the brain of rats.<sup>21</sup>

Recently, transferrin receptor–targeted dextran-coated iron oxide nanoparticles were shown to have very efficient cellular uptake and were used to follow in vivo migration of labeled oligodendrocyte neural progenitor cells after injection into rat spinal cords<sup>22</sup>; 50 000 labeled cells were injected at one site, and it is unclear what minimum number of cells localized in one area could be imaged using this contrast agent. Weissleder and coworkers linked small

dextran-coated fluorescent iron oxide particles to the tat peptide from the human immunodeficiency virus. This translocation signal increased uptake of the particles up to 100-fold into lymphocytes and other hematopoietic cells, compared with particles without tat.<sup>23</sup> Human CD34<sup>+</sup> cells labeled with these particles could be recovered from the marrow of immunodeficient mice following transplantation and detected via MRI in bones of these animals after removal of the bone from the whole mouse but not in vivo in real time following transplantation.<sup>23</sup> Most recently, Bulte and coworkers<sup>24</sup> have utilized a new contrast agent termed a magnetodendrimer, suspending iron oxide particles within a dendrimer matrix that is efficiently taken up into cells and optimized for favorable magnetic properties for imaging; 50 000 neural stem cells labeled with these particles could be detected in vivo following injection into the rat brain and used to track migration of

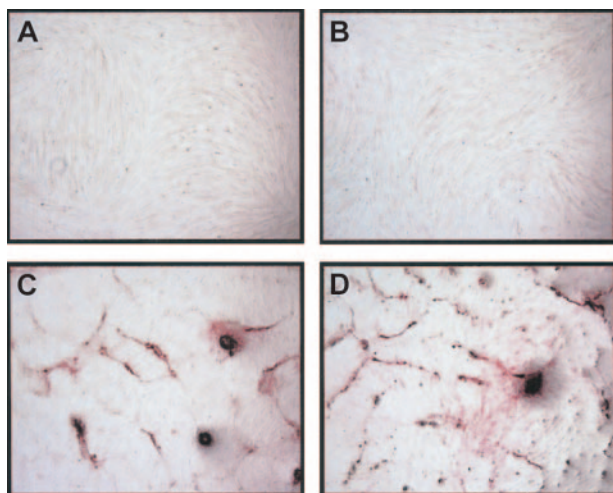


**Figure 6. Osteogenic differentiation of particle-loaded cells.** Porcine MSCs were exposed to 10 μL/mL iron particles overnight, washed and cultured under MSC conditions for 48 hours, and then changed to osteogenic induction media. After 17 days, unlabeled (A) and iron-labeled (B) cells had the same morphology in culture. Alkaline phosphatase expression and pattern were similar in unlabeled (C) and iron-labeled (D) cells. Original magnification for panels A and B, × 60; panels C and D, × 150.

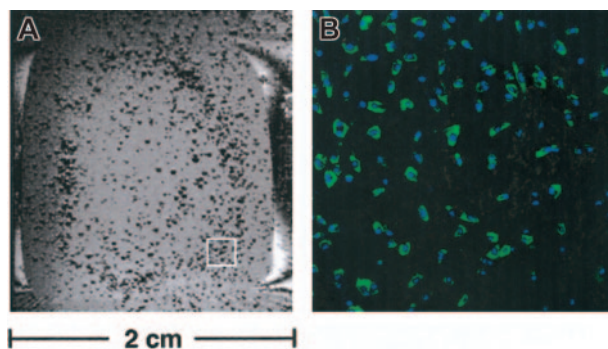


**Figure 7. Magnetic resonance imaging of live particle-loaded cells.** (A) One slice from a 3-dimensional MR data set showing a single chamber of a culture dish containing live, labeled MSCs in culture media. Single cells are present where there are dark spots in the dish, owing to the susceptibility effect of the endocytosed particles. (B) Representative confocal image of the area within the white box in panel A from the same chamber slide showing highly efficient labeling (green fluorescence) of nearly 100% of the plated cells (nuclei counterstained with DAPI). Original magnification for panel B, × 100.

the cells for up to 6 weeks. Finally, mixing ultrasmall iron oxide particles with common lipofection agents has enabled efficient labeling of stem cells and in vivo tracking in the brain.<sup>25,26</sup>

The fluorescent iron oxide polymer particles we now report offer several potential advantages for certain applications compared with previously described agents. Single cells have been detected in vitro after labeling with iron oxide, but this required very high resolutions.<sup>23,27</sup> The large particles should enable the presence of single cells to be detected at lower resolutions (200  $\mu\text{m}$ ) that can be achieved in vivo. These particles are much larger than other agents, with an average diameter of 0.9 to 1.0  $\mu\text{m}$ . Larger particles will create a much greater magnetic moment within individual cells, increasing the likelihood that in vivo imaging of single cells or very small numbers of cells will be possible. This is particularly important for studying hematopoietic stem cell homing to the marrow, because very small numbers of highly purified hematopoietic stem cells (HSCs) are used to analyze the determinants of engraftment. These particles are taken up very rapidly and with high efficiency into all cell types analyzed to date, with no apparent toxicity or impact on bioactivity, despite dense loading of the cells with large iron particles.

The  $T_2^*$  effect obtained with particle labeling was much greater than the  $T_1$  effect. To obtain reasonable  $T_1$  contrast, solvent molecules must come within close proximity of the paramagnetic center, facilitating energy transfer and relaxation back to equilibrium. This is true despite the increase in  $R_1$  relaxivity with field strength.<sup>28</sup> Evidence to this has been shown in the rather elegant example of Louie et al with "smart" gadolinium (Gd)-based contrast agents.<sup>29</sup> The poly-

mer coating of the large particles reported here most likely prevented solvent access but also protected the cell from any detrimental effects of the iron and the fluorochrome.

We have demonstrated that a variety of primary human cells of interest as vehicles for cell therapies, including hematopoietic stem cells, lymphocytes, and mesenchymal stem cells, can be efficiently labeled using fluorescent micron-scale iron oxide particles that allow ready MRI detection down to single cell resolution. The uptake of these particles does not appear to impact on the proliferative or differentiative potential of these cell populations. These new techniques may provide biologic insight into stem and progenitor cell homing and engraftment. We are currently utilizing labeled HSCs to investigate the cell surface antigens required for normal homing to the marrow and spleen following intravenous administration, and labeled MSCs delivered via direct myocardial injection or intravenously to assess whether these cells can localize and contribute to myocardial regeneration following infarction. We are additionally investigating the effect of magnetic label dilution and the effect it has on cell visualization.

## Acknowledgments

We are grateful to Zu-Xi Yu from the Core Electron Microscopy Facility, Kevan Keyvanfar for flow cytometry, Robert Lederman for helpful comments, and Ilsa Rovira for technical assistance with manuscript preparation.

## References

- Lapidot T. Mechanism of human stem cell migration and repopulation of NOD/SCID and B2mnull NOD/SCID mice. The role of SDF-1/CXCR4 interactions. *Ann N Y Acad Sci*. 2001;938:83-95.
- Lagasse E, Connors H, Al-Dhalimy M, et al. Purified hematopoietic stem cells can differentiate into hepatocytes in vivo. *Nat Med*. 2000;6:1229-1234.
- Orlic D, Kajstura J, Chimenti S, Bodine DM, Leri A, Anversa P. Transplanted adult bone marrow cells repair myocardial infarcts in mice. *Ann N Y Acad Sci*. 2001;938:221-229; discussion 229-230.
- Orlic D, Kajstura J, Chimenti S, et al. Bone marrow cells regenerate infarcted myocardium. *Nature*. 2001;410:701-705.
- Takahashi T, Kalka C, et al. Ischemia- and cytokine-induced mobilization of bone marrow-derived endothelial progenitor cells for neovascularization. *Nat Med*. 1999;5:434-438.
- Toma C, Pittenger MF, Cahill KS, Byrne BJ, Kessler PD. Human mesenchymal stem cells differentiate to a cardiomyocyte phenotype in the adult murine heart. *Circulation*. 2002;105:93-98.
- Jiang Y, Jahagirdar BN, Reinhardt RL, et al. Pluripotency of mesenchymal stem cells derived from adult marrow. *Nature*. 2002;418:41-49.
- Lanzkron SM, Collector MI, Sharkis SJ. Hematopoietic stem cell tracking in vivo: a comparison of short-term and long-term repopulating cells. *Blood*. 1999;93:1916-1921.
- Hardy J, Edinger M, Bachmann MH, Negrin RS, Fathman CG, Contag CH. Bioluminescence imaging of lymphocyte trafficking in vivo. *Exp Hematol*. 2001;29:1353-1360.
- Adonai N, Nguyen KN, Walsh J, et al. Ex vivo cell labeling with  $^{64}\text{Cu}$ -pyruvaldehyde-bis(N4-methylthiosemicarbazone) for imaging cell trafficking in mice with positron-emission tomography. *Proc Natl Acad Sci U S A*. 2002;99:3030-3035.
- Allport JR, Weissleder R. In vivo imaging of gene and cell therapies. *Exp Hematol*. 2001;29:1237-1246.
- Pittenger MF, Mackay AM, Beck SC, et al. Multilineage potential of adult human mesenchymal stem cells. *Science*. 1999;284:143-147.
- Berenson RJ, Bensinger WI, Hill RS, et al. Engraftment after infusion of CD34+ marrow cells in patients with breast cancer or neuroblastoma. *Blood*. 1991;77:1717-1722.
- Reyes M, Verfaillie CM. Characterization of multipotent adult progenitor cells, a subpopulation of mesenchymal stem cells. *Ann N Y Acad Sci*. 2001;938:231-233; discussion 233-235.
- Hawrylak N, Ghosh P, Broadus J, Schlueter C, Greenough WT, Lauterbur PC. Nuclear magnetic resonance (NMR) imaging of iron oxide-labeled neural transplants. *Exp Neurol*. 1993;121:181-192.
- Jacobs RE, Fraser SE. Magnetic resonance microscopy of embryonic cell lineages and movements. *Science*. 1994;263:681-684.
- Bulte JW, Hoekstra Y, Kamman RL, et al. Specific MR imaging of human lymphocytes by monoclonal antibody-guided dextran-magnetite particles. *Magn Reson Med*. 1992;25:148-157.
- Bulte JW, Ma LD, Magin RL, et al. Selective MR imaging of labeled human peripheral blood mononuclear cells by liposome mediated incorporation of dextran-magnetite particles. *Magn Reson Med*. 1993;29:32-37.
- Yeh TC, Zhang W, Ildstad ST, Ho C. Intracellular labeling of T-cells with superparamagnetic contrast agents. *Magn Reson Med*. 1993;30:617-625.
- Yeh TC, Zhang W, Ildstad ST, Ho C. In vivo dynamic MRI tracking of rat T-cells labeled with superparamagnetic iron-oxide particles. *Magn Reson Med*. 1995;33:200-208.
- Franklin RJ, Blaschuk KL, Bearchell MC, et al. Magnetic resonance imaging of transplanted oligodendrocyte precursors in the rat brain. *Neuroreport*. 1999;10:3961-3965.
- Bulte JW, Zhang S, van Gelderen P, et al. Neurotransplantation of magnetically labeled oligodendrocyte progenitors: magnetic resonance tracking of cell migration and myelination. *Proc Natl Acad Sci U S A*. 1999;96:15256-15261.
- Lewin M, Carlesso N, Tung CH, et al. Tat peptide-derivatized magnetic nanoparticles allow in vivo tracking and recovery of progenitor cells. *Nat Biotechnol*. 2000;18:410-414.
- Bulte JW, Douglas T, Witwer B, et al. Magnetodendrimers allow endosomal magnetic labeling and in vivo tracking of stem cells. *Nat Biotechnol*. 2001;19:1141-1147.
- Hoehn M, Kustermann E, Blunk J, et al. Monitoring of implanted stem cell migration in vivo: a highly resolved in vivo magnetic resonance imaging investigation of experimental stroke in rat. *Proc Natl Acad Sci U S A*. 2002;99:16267-16272.
- Frank JA, Zywicke H, Jordan EK, et al. Magnetic intracellular labeling of mammalian cells by combining (FDA-approved) superparamagnetic iron oxide MR contrast agents and commonly used transfection agents. *Acad Radiol*. 2002;9(suppl 2):S484-S487.
- Dodd SJ, Williams M, Suhan JP, Williams DS, Koretsky AP, Ho C. Detection of single mammalian cells by high-resolution magnetic resonance imaging. *Biophys J*. 1999;76:103-109.
- Lauffer RB. Paramagnetic metal-complexes as water proton relaxation agents for NMR imaging—theory and design. *Chem Rev*. 1987;87:901-927.
- Louie AY, Huber MM, Ahrens ET, et al. In vivo visualization of gene expression using magnetic resonance imaging. *Nat Biotechnol*. 2000;18:321-325.